ESTIMATION OF POLLUTANT DISPERSION AROUND A BUILDING WITHIN NON-ISOTHERMAL BOUNDARY-LAYER USING DETACHED EDDY SIMULATION

by

Svetlana VALGER*

Khristianovich Institute of Theoretical and Applied Mechanics SB RAS, Novosibirsk, Russia

Original scientific paper
https://doi.org/10.2298/TSCI211123046V

The paper presents the numerical results of modelling pollutant transport from a low source behind a bluff-body imitating a building within a non-isothermal boundary-layer. The main goal of the study is to estimate the tracer gas dispersion in a complex turbulent separated flow behind a building in the presence of interference of the atmospheric boundary-layer and local flows. In the fist part of the study we compare numerical approaches URANS and IDDES for turbulent flow prediction on a configuration for which experimental data are available. It is shown that detached eddy simulation approach predicts correctly the main separated flow features and demonstrates a reliable correlation with the experimental data on mean velocity, pollutant concentration and temperature fields. In the second part of the study, the influence of unstable thermal stratified flow on the tracer gas transport around a building is analyzed using IDDES method. The unstable thermal flow regime considered in the study affects the distribution of the pollutant concentration in the re-circulation zone behind the building. The presence of additional buoyancy effects leads to an increase in the gas concentration on the leeward wall of the body and gas transport from a ground region to a height greater than in the case with the neutral boundary-layer.

Key words: *pollutant dispersion, unstable thermal stratification, building aerodynamics, detached eddy simulation, urban environmental problems*

Introduction

We now have credible data that prove that air pollutants as toxic gases and micro-particles have a negative influence both on the environment and human health. According to the WHO's 2021 report *Global Air Quality Guidelines. Particulate matter (PM2.5 and PM10), ozone, nitrogen dioxide, sulfur dioxide and carbon monoxide* [1], about 7 million people per year die of non-infectuous diseases caused air pollution. High concentration of air pollutants may lead to coronary strokes, heart and lung conditions, severe and chronic respiratory diseases. Air pollution is among the top five global risks for global health out of the 87 factors rated in the study [2]. The main contributors to air pollution are antropogenic factors such as fuel combustion, transport exhaust, industrial airborne waste, *etc.* In large cities with well-developed infrastructures transport exhaust makes a considerable contribution to lower air quality [3]. Campaigns for air quality improvement are accompanied by research into iden-

* Authors' e-mail: valger@itam.nsc.ru

tifying the sources of pollutants and developing measures to reduce their quantity [4-6] as well as monitoring their levels, in situ observations and data analysis [7-9].

Experimental research and numerical modelling research play an important part in studying the fundamental mechanisms of pollutant dispersion in city environments. Among all the experimental publications that are based various small-scale models of buildings and city fragments, one must note benchmarking that allows studying physical processes in the flow and serves as a basis for validation of numerous numerical models. The series of experiments conducted by Gromke and Ruck [10] is devoted to studying isotermic transfer of gas pollutants in street canyons with a focus on the effect of green spaces. Yoshie *et al.* [11] demonstrates the results of the experiments that describe isotermic and non-isotermic air flows in the vicinity of standalone bodies and their systems that imitate in-built city areas with consideration for mass transfer of gas pollutants from low-standing sources. The articles [12-14] are devoted to experimental data on microclimactic parameters in the vicinity of various urban settings (a street canyon model, a system of cubical buildings, a system of buildings of varied height, *etc.*). It should be noted that experimental research conducted on small-scale models does not always reproduce the flow dynamics for full-scale configurations correctly due to its inability to adhere to similarity criteria; this is extensively explained in the review conducted by Zhao *et al.* [15]. Numerical simulation can model the flow structure in urban settings in its full scale, which appears to be an important advantage of these methods. However, validation of the chosen methods of numerical simulation is a primary challenge. Publications [16-18] include guidelines for numerical simulation. However, methods for numerical simulation of thermally stratified flows in the vicinity of buildings and building complexes with consideration for mass transfer of gas pollutants are still underesearched. The main challenges in this area are development of guidelines for practical calculation of non-isotermic flows in the vicinity of buildings, analysis of non-stationary heat processes on the basis of large/detached eddy simulation approaches to turbulence modelling, describing the flow configurations where buoyancy effects start to affect pollutant dispersion considerably, *etc.* For instance, meta-analysis of the existing data [15, 19] demonstrate that the LES/DES approaches are more rarely applied to urban aerodynamics tasks with consideration for microclimatic processes if we compare them with the common RANS/URANS semi-empirical models. At the same time, RANS/URANS approaches do not allow us to calculate turbulent flow characteristics in a correct manner, for instance, when applied to predicting the size of boundary-layer separation zones and recirculation zones that appear in flows around buildings and street canyons [20-22].

The present research has two objectives. First of all, we aim to acquire data on detached eddy simulation approaches application and to specify the methodology of numerical simulation for the problem of gas pollutant transfer in the vicinity of a building with a complex flow physics (taking into account the thermal physics). The experimental benchmark [11] allows us to validate the IDDES k-ω SST numerical approach and compare it with the widely-used URANS k-ω SST approach. Solving this problem is part of the validation research that aims to establish which approaches are more effective for outdoor pollution problems. The author considers accumulation of these data to be an important step for incorporating these approaches into practical modelling for environmental and civil engineering aerodynamics problems. The second objective is to describe the physics of a flow with consideration for unstable thermal stratification of boundary-layer and mass transfer of heavy gas as a pollutant source. The author aims to evaluate the contribution of unstable stratification into tracer gas dispersion in a separation flow with a complex structure formed around a building-like prysm fixed on a flate plate.

Problem statement

The problem under consideration is flow of a gas mixture around a prism with the aspect ratio of 1:1:2 in the presence of a gas pollutant source located on the ground surface behind the prism. The problem statement reproduces the conditions of the experimental benchmarks [11] performed in the thermally stratified wind tunnel of Tokyo Polytechnic University, which allows to validate numerical models and methods. The scheme of the computational domain is shown in the fig. 1. We consider a prism with a height $h = 0.16$ m and a width $b = 0.5h$ fixed on the flat plate. The tracer gas is 5% C_2H_4 and it is injected into the air through the circular hole with the diameter $d = 5\cdot10^{-3}$ m located on the ground at the distance of $0.25h$ from the leeward side of the prism. The computational domain size is $11h\times7h\times5.625h$ and it is chosen based on the data about the wind tunnel characteristics and using recommendations presented in [23, 24].

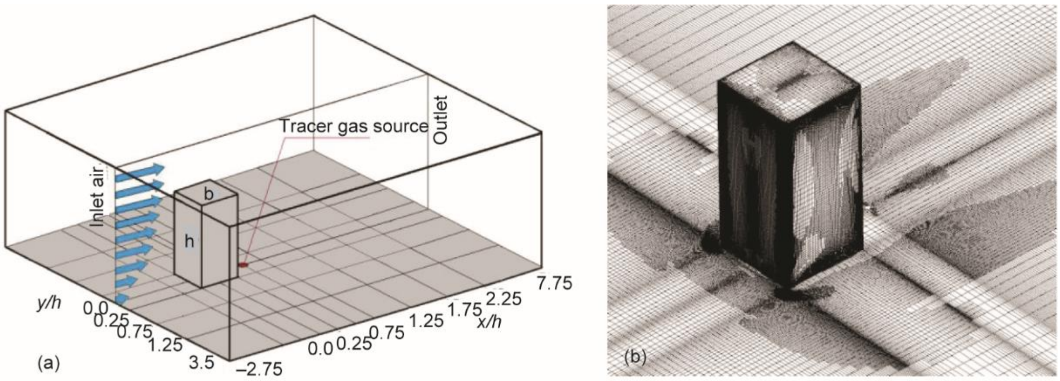

Figure 1. The computational domain (a) and the grid on walls of the prism and ground (b) used in the calculations

The tracer gas is injected into the domain at the flow rate of $q = 9.17\cdot10^{-6}$ m^3/s. We analyze two thermal regimes imitating atmospheric boundary-layer conditions. The first regime (Case 1) corresponds to unstable thermal stratification of the boundary-layer and the second regime (Case 2) describes neutral thermal conditions close to isothermal. The tracer gas is supplied to the domain at the temperature $\langle T_g\rangle = 30.4$ °C and $\langle T_g\rangle = 21.2$ °C for Case 1 and Case 2, respectively. The two considered cases also differ in their temperature conditions on the ground $\langle T_f\rangle$, the prism walls $\langle T_b\rangle$ and at the inlet boundary. The boundary and flow conditions for both cases are defined in tab. 1. The bulk Richardson number, calculated as $\mathrm{Ri_b} = gh(\langle T_h\rangle - \langle T_f\rangle)/[(\langle T_0\rangle + 273)\langle U_h\rangle^2]$, where $g = 9.81$ m/s^2 is the acceleration of gravity, $\langle T_h\rangle$ [°C] and $\langle U_h\rangle$ [ms^{-1}] – air temperature and mean air velocity at height h [m] at the inlet boundary, $\langle T_0\rangle$ [°C] – space averaged air temperature, is $\mathrm{Ri_b} \approx -0.085$ for Case 1 and $\mathrm{Ri_b} \approx 0.0$ for Case 2.

At the inlet boundary of the computational domain, the air flow is described by profiles of mean velocity, fig. 2(a) and turbulent kinetic energy (TKE), fig. 2(b) corresponding to the experimental data [11]. The flow Reynolds number calculated using the inlet mean air velocity, U_h, at the height h is $\mathrm{Re}_{Uh} \approx 1.6 \cdot 10^4$. The vertical air temperature gradient is set in accordance with the profile shown in fig. 2(c), for the Case 1.

Table 1. Boundary and flow conditions

Parameter	Unstable non-isothermal state (Case 1)	Isothermal state (Case 2)
Mean velocity of inlet air at height h, $<U_h>$ [ms^{-1}]	1.46	1.46
Ground surface temperature, $<T_f>$[°C]	45.8	21.2
Inlet air temperature at height h, $<T_h>$ [°C]	12.2	21.5
Absolute value of temperature difference, $<\Delta T> = \vert<T_h> - <T_f>\vert$ [°C]	33.6	0.4
Prism surface temperature, $<T_b>$ [°C]	24.5	21.1
Temperature of injected tracer gas, $<T_g>$ [°C]	30.4	21.2
Space averaged air temperature, $<T_0>$ [°C]	16.6	21.5
Injected tracer gas concentration, C_g [ppm]	$5 \cdot 10^4$	
Tracer gas flow rate at injector, q [m^{3}s^{-1}]	$9.17 \cdot 10^{-6}$	
Bulk Richardson number, Ri_b [–]	–0.085	0.00

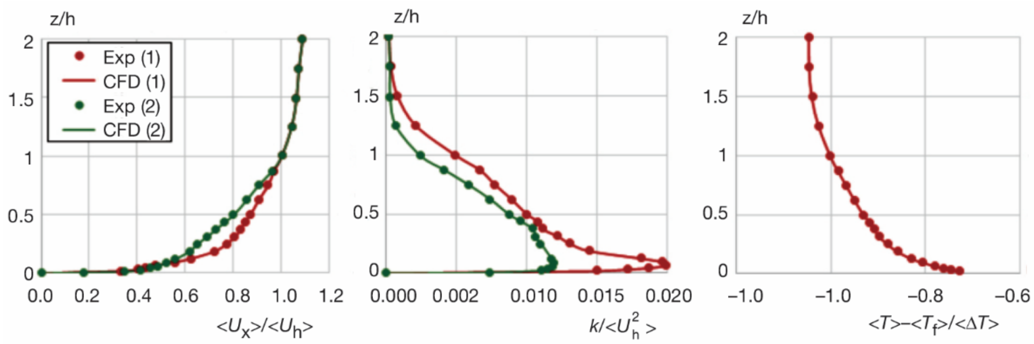

Figure 2. The boundary conditions profiles of inlet air used in experiment [11] (Exp.) and calculations (CFD) within the unstable non-isothermal (1) and isothermal boundary-layer (2); (a) – mean velocity $<U>/<U_h>$, (b) – TKE $k/<U_h>^2$, and (c) – mean temperature $(<T> - <T_f>)/<\Delta T>$

Mathematical model and methods

At the stage of model validation, two approaches are chosen to describe turbulence: the *k-ω* SST model based on solving Reynolds averaging of governing equations [25] and the hybrid eddy-resolving approach IDDES *k-ω* SST [26], which allows to improve the DES approach [27, 28] for the case of calculating reattached flows. The considered numerical model is based on the 3-D unsteady Reynolds-averaged Navier-Stokes equations, suplemented by convection-diffusion equation for the mass fraction of ethylene [29]:

$$\frac{\partial \rho}{\partial t} + \nabla(\rho \vec{\mathrm{U}}) = 0 \tag{1}$$

$$\frac{\partial}{\partial t}(\rho\vec{U}) + \nabla(\rho\vec{U}\vec{U}) = -\nabla p + \nabla(\tau_m + \tau_t) + \rho\vec{g} \tag{2}$$

$$\frac{\partial}{\partial t}(\rho Y) + \nabla(\rho\vec{U}Y) = -\nabla\vec{J}, \quad \vec{J} = -\left(\rho D_m + \frac{\mu_t}{Sc_t}\right)\nabla Y - D_T\frac{\nabla T}{T} \tag{3}$$

Equations (1)-(3) are described in averaged variables, where ρ is the density of the mixture, $\vec{U}$ – the velocity vector of the averaged flow with components U_x, U_y, and U_z, p – the pressure, and T – the temperature.

$$\tau_m = 2\mu\left\{\frac{1}{2}[\nabla\vec{U} + (\nabla\vec{U})^T] - \frac{1}{3}I\nabla\vec{U}\right\} \quad \text{and} \quad \tau_t = 2\mu_t\left\{\frac{1}{2}[\nabla\vec{U} + (\nabla\vec{U})^T] - \frac{1}{3}I\nabla\vec{U}\right\} + \frac{2}{3}kI$$

are the molecular and turbulent components of the viscous stress tensor, μ and μ_t are the molecular and turbulent viscosity, $\vec{g}$ – the gravitational acceleration vector, Y – the local mass fraction of ethylene, $\vec{J}$ – the diffusion flux of ethylene; D_m and D_T – the mass and thermal diffusion coefficients for ethylene, the turbulent Schmidt number is $Sc_t = 0.7$, k – the turbulence kinetic energy, and I – the unit tensor.

The incompressible ideal gas law is used to define mixture density as a function of temperature [29]:

$$\rho = \frac{P_0}{RT\sum_i \frac{Y_i}{M_{w,i}}}$$

where R is the universal gas constant, $M_{w,i}$ – the molecular weight of species i, $P_0 = 1$ atm.

The energy equation is described in the follow form:

$$\frac{\partial}{\partial t}(\rho E) + \nabla(\rho\vec{U}H) = \nabla[\vec{U}(\tau_m + \tau_t) + (\vec{q}_m + \vec{q}_t)] \tag{4}$$

where the total energy $E = C_v T + 0.5(U_x^2 + U_y^2 + U_z^2)$, the total enthalpy $H = E + p/\rho = C_p T + 0.5(U_x^2 + U_y^2 + U_z^2)$, $\vec{q}_m = -\lambda\nabla T$ and $\vec{q}_t = -\lambda_t\nabla T$ – the molecular and turbulent components of the heat flux density vector, λ – the thermal conductivity coefficient, $\lambda_t = (C_p\mu_t)/Pr_t$ – the turbulent thermal conductivity for mixture of gases, C_v and C_p – the specific heat at constant volume and at constant pressure for mixture of gases, and $Pr_t = 0.85$.

The general form of equations in k-ω SST model [25] describing turbulent effects in the flow is:

$$\frac{\partial}{\partial t}(\rho k) + \frac{\partial}{\partial x_i}(\rho k v_i) = \frac{\partial}{\partial x_j}\left(\Gamma_k \frac{\partial k}{\partial x_j}\right) + G_k - R_k + G_b \tag{5}$$

$$\frac{\partial}{\partial t}(\rho\omega) + \frac{\partial}{\partial x_i}(\rho\omega v_i) = \frac{\partial}{\partial x_j}\left(\Gamma_\omega \frac{\partial\omega}{\partial x_j}\right) + G_\omega - R_\omega + G_{\omega b} \tag{6}$$

where G_k is the production of turbulence kinetic energy k, G_ω – the generation of the specific dissipation rate ω, Γ_k and Γ_ω – the effective diffusivity of k and ω, respectively, R_k and R_ω – the dissipation of k and ω, respectively, and G_b and $G_{\omega b}$ – the buoyancy terms [25, 29]. The turbulence model (5-6) is widely used today to solve applied issues of building aerodynamics, for example, to predict the wind load on facades or to assess pedestrian comfort near buildings [30, 31].

In eq. (5), the dissipation term R_k is defined as $R_k = \rho\beta^*\omega k$ for the k-ω SST model, where $\beta^* = 0.09$, and as $R_k = \rho\sqrt{k^3}/l_{\mathrm{IDDES}}$ for the IDDES SST model [26].

Thus, the IDDES model is based on replacement of turbulent length scale l_{RANS}, which is defined as $k^{1/2}/\beta^*\omega$ in k-ω SST model, for the hybrid length scale:

$$l_{\mathrm{IDDES}} = \tilde{f}_d(1+f_e)l_{\mathrm{RANS}} + (1-\tilde{f}_d)l_{\mathrm{LES}} \tag{7}$$

where LES grid length scale $l_{\mathrm{LES}} = C_{\mathrm{DES}}\Psi\Delta$, where $C_{\mathrm{DES}} = 0.61$ is empirical constant and Ψ is a low-Reynolds number correction [32]. The length scale l_{LES} is calculated using the local grid cell size and the distance from the wall to the current coordinate:

$$\Delta = \min\left[\max(C_{\mathrm{w}}d_{\mathrm{w}}, C_{\mathrm{w}}h_{\max}, h_{\mathrm{wn}}), h_{\max}\right] \tag{8}$$

where (8), $h_{\max}$ is the maximal grid cell scale in the considered point of the domain, h_{wn} – the grid cell size in the direction normal to the wall, d_{w} – the wall distance and $C_{\mathrm{w}} = 0.15$. In eq. (1) $\tilde{f}_d$ and f_{e} are empirical constants defined in [26] in detail and used for the correct calculation of RANS and DDES regions.

The problem is solved using the FLUENT 2020R1 software [29] by the finite volume method. We use the computational grid including hexahedral elements. The condition $y + <1$ is achieved by adapting the computational grid using additional sublevels of computational cells, fig. 1(b). To estimate the grid convergence of the solution, preliminary calculations were carried out on three grids differing in the size of cell. The total number of cells in the considered grids was ≈ 2.1 million, ≈ 4.7 million, and ≈ 14.4 million, respectively. A total number of elements of ≈ 14.4 million was the maximal under the conditions of the available computational resources. The mean length of the separation zone x_{r}/h located behind the prism and calculated for the central section ($y = 0$ m) was chosen as a parameter for estimating the solution convergence. As can be seen from fig. 3(a), for two more detailed grids, fairly close values of x_{r}/h are observed, however, the grid convergence has not been fully achieved. Analyzing these results, in further calculations, the most detailed computational grid of ≈14.4 million cells is used.

The bounded central differencing scheme is used for the spatial approximation of momentum equations and second oder upwind scheme is used to the approximate transport equations for turbulence, species and energy. For the temporal approximation of the governing equations, an implicit scheme of the second order of accuracy was used. To achieve the convergence of the solution at each time step, the criterion for achieving the absolute values of the residuals for energy equation was $\approx 10^{-6}$ and it was $\approx 10^{-4}$ for other variables. Calculations are performed with the time step $\tau U_{\mathrm{h}}/h \approx 4.56 \cdot 10^{-3}$. The period of time averaging the variable fields is chosen using recommendations [20] and equal to $\Delta t U_{\mathrm{h}}/h \approx 200$.

The boundary conditions at the inlet boundary of the computational domain, fig. 1(a), are set as profiles of mean velocity, mean temperature (for Case 1) and TKE, fig. 2, calculated by cubic spline interpolation of the experimental data [11]. For Case 2, the inlet temperature of airflow $T = 21.5$ °C is constant over the height of the computational domain. To calculate the profile of the TKE specific dissipation rate, we use the relation $\omega = \varepsilon/(k\beta^*)$, $\varepsilon = (C_\mu^{0.75}k^{1.5})/l$, $C_\mu = 0.09$, where l is the characteristic length [20]. In IDDES simulation, the vector of turbulent pulsations is calculated as a superposition of amplitude-modulated Fourier modes based on the synthetic turbulence generation method [33].

On the ground wall and the prism walls, the no-slip condition of a smooth wall ($U_{\mathrm{x}} = U_{\mathrm{y}} = U_{\mathrm{z}} = 0$) with a fixed temperature corresponding to the experimental data is set, tab. 1. The outer boundaries of the computational domain are located in such a way as to ensure the absence of their influence on the flow field in the vicinity of the prism. We use the symmetry condition, which ensures zero velocity and zero gradients of the variables along the normal to the boundary, at the lateral ($y = 3.5h$;$-3.5h$) and upper ($z = 5.625h$) domain boundaries. At the outlet boundary of the computational domain ($x = 7.75h$), the condition of constant static pressure $\Delta P = P_{st} - P_0 = 0$ atm is set.

In experimental data [11], the mean velocity, TKE, tracer gas concentration and temperature profiles in the characteristic sections around the prism were presented, so the considered benchmark makes it possible to validate the turbulence model as applied to the prediction of a complex separated flow under a non-isothermal airflow regime.

Result analyses and discussions

Turbulence model validation

At the first stage, we compare the numerical results for Case 1 obtained using two turbulence models URANS k-ω SST (hereinafter referred to as URANS) and IDDES k-ω SST (hereinafter referred to as IDDES). In fig. 3(b), the isobars of Q-criterion = 1300 s^{-2} colored with value of flow mean velocity $\langle U_x \rangle / \langle U_h \rangle$ obtained using IDDES are shown. From the point of view of pollutant gas dispersion is the vortex zone – 1, behind the prism, where the tracer gas injected from the ground, represents the biggest interest. The study [22] described the isothermal case of a flow around a prism with a size ratio 2:1:1 fixed on a flat plate and found that the RANS approach underestimates the TKE level in zone – 1, which leads to a significant overestimation of the longitudinal size of the separation zone behind the prism. In addition, application of this approach to assess pollutant dispersion around buildings is often difficult in terms of choosing semi-empirical constants of the turbulence model [34, 35]. It was shown in [35] that the turbulent Schmidt number, Sc_t, has a large effect on the accuracy of predicting the pollutant transport and there is no universal values for the problems of buildings aerodynamics, where a complex interference of atmospheric flow and local flows forming around building is observed. In our calcualtions, the turbulent Schmidt number $Sc_t = 0.7$ is set, which is used by default in FLUENT for a wide range of problems.

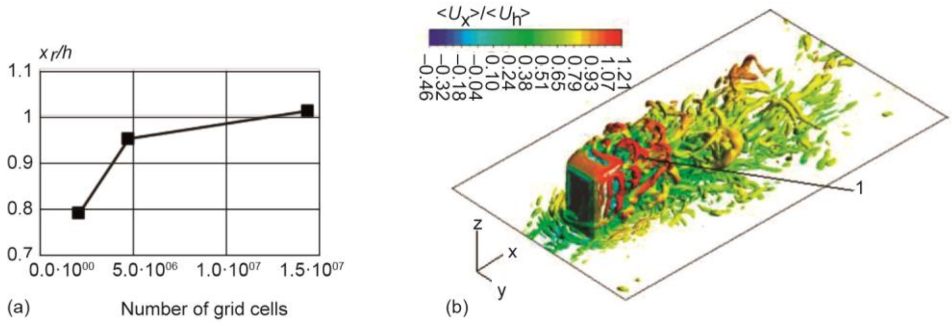

Figure 3. Grid convergence analysis (a) and isobars of Q-criterion = 1300 s^{-2} colored with value of flow mean velocity $\langle U_x \rangle / \langle U_h \rangle$ (b)

In figs. 4(a)-4(c) the mean velocity $\langle U_x \rangle / \langle U_h \rangle$ fields in the central plane ($y = 0$ m) are shown. They were obtained using the URANS and IDDES turbulence models. The contour black line in the figures denotes the isoline $\langle U_x \rangle = 0$. The two models show significant differences in determining the size of the separation zone behind the prism. The calculation using the URANS approach, fig. 4(c) predicts the extended separation zone – 1, with dimensions of ≈2h behind the prism, while in the IDDES calculation, fig. 4(a), the length of the zone – 1, is significantly less and is ≈ h. In the angle between the leeward side of the prism and the ground, in both calculations, a secondary corner flow – 2, is formed with a maximum height $h_{sf} \approx 0.045h$ in the IDDES calculation and $h_{sf} \approx 0.11h$ in the URANS calculation. The length of the separation zone – 3, on the top of the prism is $h_{sz} \approx 0.32h$ (IDDES) and $h_{sz} \approx 0.4h$ (URANS) in the central section.

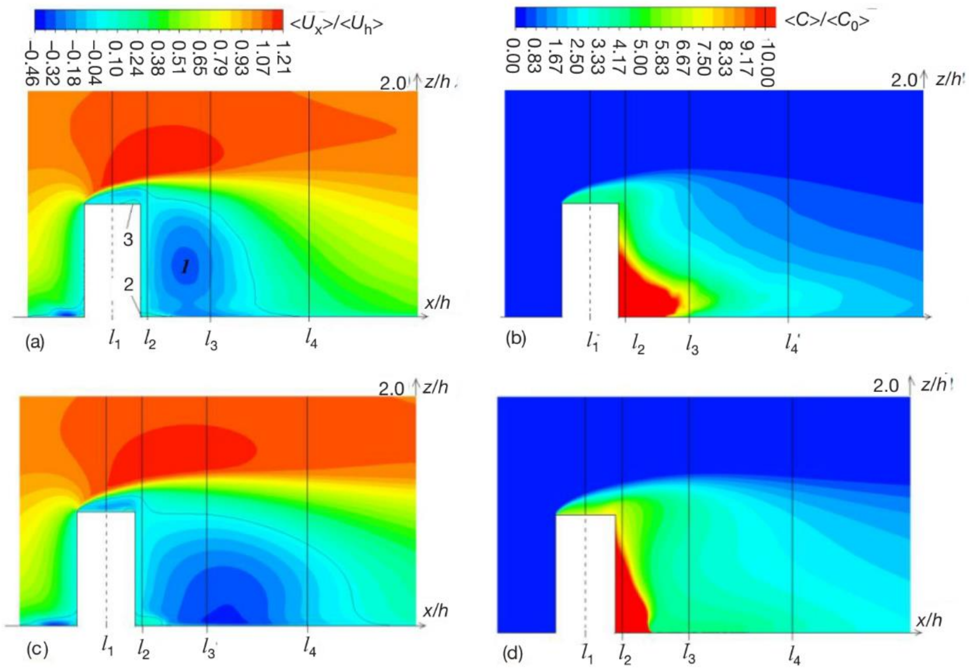

Figure 4. Mean *x*-velocity $<U_x>/<U_h>$ (a, c) and mean tracer gas concentration $<C>/C_0$ (b, d) fields at the central pane (y = 0 m) calculated for the Case 1 using IDDES *k-ω* SST (a, b) and URANS *k-ω* SST (c, d) approaches

The profiles of the mean velocity $<U_x>/<U_h>$ obtained in the calculations and the experiment [11] along the lines $l_1 = 0$ 5(a), $l_2 = 0.3125h$ 5(b), $l_3 = 0.875h$ 5(c), and $l_4 = 1.75h$ 5(d) in the central plane (y = 0 m), are demonstrated in fig. 5. For the lines l_1 and l_2, both the numerical models predict the velocity distribution accurately. However, in the separation zone behind the prism and at a distance from the leeward wall of the prism (lines l_3 and l_4), the IDDES approach allows one to obtain better agreement with the experimental data and correctly predict the flow reattachment zone.

Fields of the mean normalized ethylene concentration $<C>/C_0$ in the central plane (y = 0 m), where $C_0 = C_g q/(<U_h>h^2)$, figs. 4(b), and 4(d), show zones of high and low concentrations of the tracer gas. Ethylene enters the separation zone – 1, behind the prism and is transferred to the leeward wall of the prism. In both the calculations, high concentrations are observed along the leeward wall, and some of the ethylene flows to the top of the prism. For the line l_1, located above the top of the prism, fig. 5(a), both the models qualitatively describe

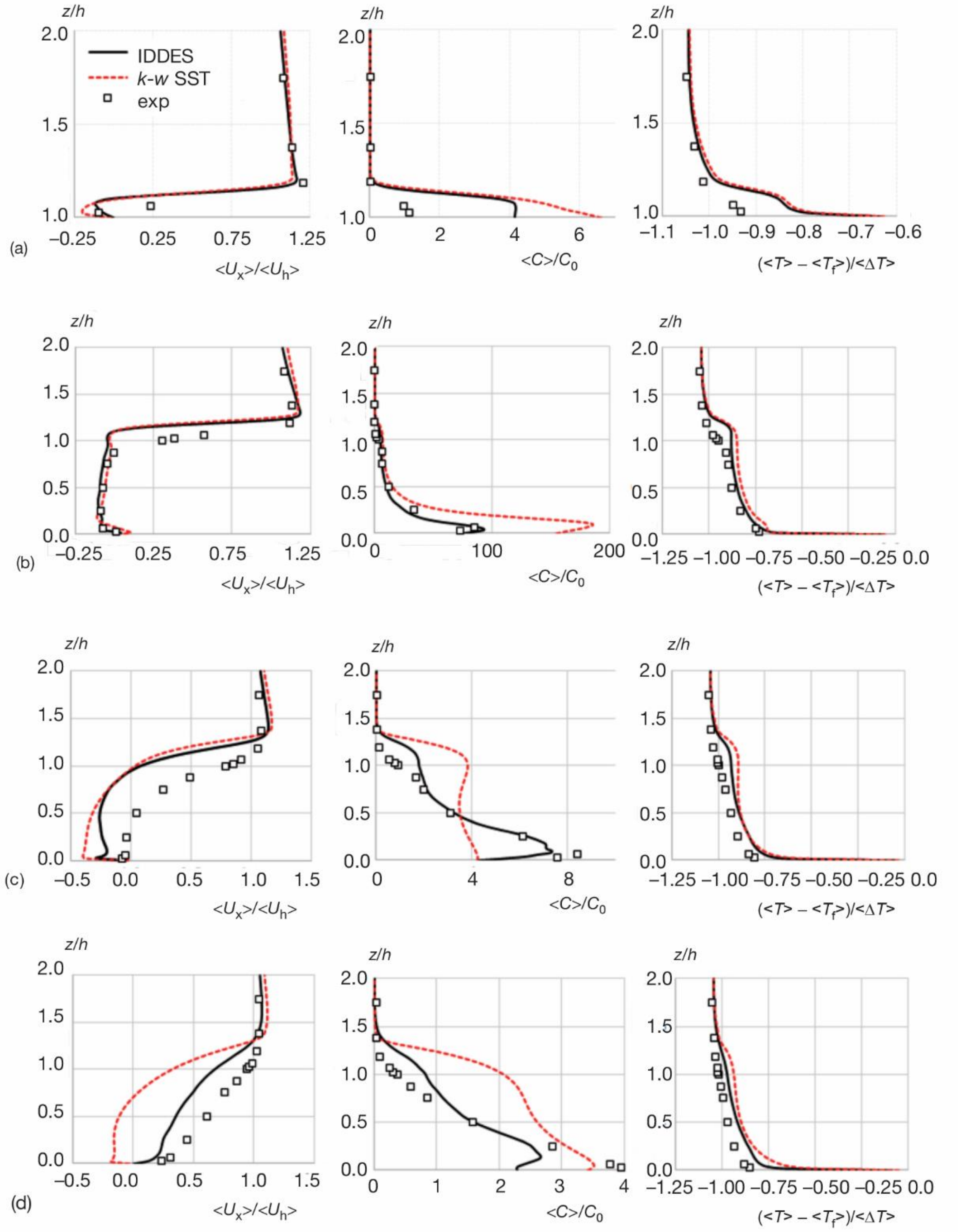

Figure 5. Profiles of mean *x*-velocity <U_x>/<U_h>, mean tracer gas concentration <*C*>/C_0 and mean temperature (<*T*> – <T_f>)/<Δ*T*> calculated for Case 1 using IDDES *k-ω* SST (---) and URANS *k-ω* SST (- - -) approaches and obtained in experiment [11] (□) along lines *x* = 0 (a), 0.3125*h* (b), 0.875*h* (c), and 1.75*h* (d) at the central plane (*y* = 0 m)

the gas concentration distribution in accordance of the experiment, but slightly overestimate its values. It indicates that numerical simulation predicts a more intense mass exchange between the zone – 3, above the prism roof and the separation zone – 1, behind the prism. In fig. 5(b), we see that along the leeward wall of the prism (line l_2) the URANS approach overestimates the ethylene concentration near the ground by almost two times, which may be associated with an incorrect prediction of the secondary corner flow –2.

For the line l_3, located in the wake of the flow behind the injector, the URANS approach does not agree with the experimental data, while IDDES predicts ethylene concentrations well, fig. 5(c). For the line l_4, the ethylene concentrations are rather low and the IDDES approach allows a qualitative description of the concentration distribution along the height, but it does not predict the concentration level near the ground exactly. The URANS approach does not provide satisfactory qualitative and quantitative agreement with the experiment on the concentration profiles.

The comparison of mean temperature profiles in characteristic sections, fig. 5, showed that both the models adequately reproduce the thermal regime as it was obtained in the experiment. It should be noted that in both the models, a higher heat transfer is observed in the shear layer between the external flow and zones – 3, in comparison of the experiment. As a conclusion of this section, we can conclude that the numerical simulation using the IDDES k- ω SST model predict good qualitatively and quantitatively the pollutant dispersion in a complex turbulent flow around the prism. In the next subsection, a comparison of IDDES simulation results for Cases 1 and 2 in tracer gas concentration fields will be disscused.

Influence of non-isothermal stratification on pollutant dispersion

In this subsection, we discuss the results of the numerical simulations based on the IDDES approach obtained for the case of unstable (Case 1) and neutral (Case 2) thermal stratification of the boundary-layer. The characteristic features of the flow behind the prism and pollutant transport for Case 1 have been described in section *Turbulence model validation*. The main goal of this subsection is to describe the effect of unstable stratification of the boundary-layer on the tracer gas dispersion in the wake behind a bluff body.

Figure 6 shows the distributions of the mean normalized concentration $\langle C\rangle/C_0$ for Cases 1 and Case 2 in characteristic cross-sections $x = 0.3125h$ 6(a), $0.625h$ 6(b), h 6(c), $2h$ 6(d), $4h$ 6(e), and $6h$ 6(f). For all the cross-sections, it is observed that the ethylene cloud has a qualitatively similar form in both cases. However, in the first considered cross-section ($x = 0.3125h$) higher ethylene concentrations are observed near the ground for Case 1. In the other cross-sections located behind the injector position, on the contrary, higher concentrations of ethylene near the ground are observed for Case 2. Based on the analysis of fig. 6, the unstable thermal stratification conditions lead to a more intense transfer of ethylene to the leeward wall of the prism, the ethylene transfer to the increased height above the prism and a significant decrease in the ethylene concentration along the ground behind the injector.

To quantitatively estimate the influence of an unstable thermal regime (Case 1) on pollutant dispersion behind the prism, the profiles of $\langle C_{\text{Case1}}\rangle/\langle C_{\text{Case2}}\rangle$, expressing the ratio of normalized ethylene concentrations obtained for Cases 1 and 2, were calculated, fig. 7. The profiles of $\langle C_{\text{Case1}}\rangle/\langle \mathrm{C}_{\text{Case2}}\rangle$ are plotted along the horizontal lines $z = 0.0625h$, $0.5h$, $0.75h$, h, $1.125h$ in the central section ($y = 0$ m). As it is shown in fig. 7, higher ethylene concentrations ($\langle C_{\text{Case1}}\rangle/\langle \mathrm{C}_{\text{Case2}}\rangle > 1$) on the leeward wall of the prism ($x/h = 0.25$) are observed in the Case 1

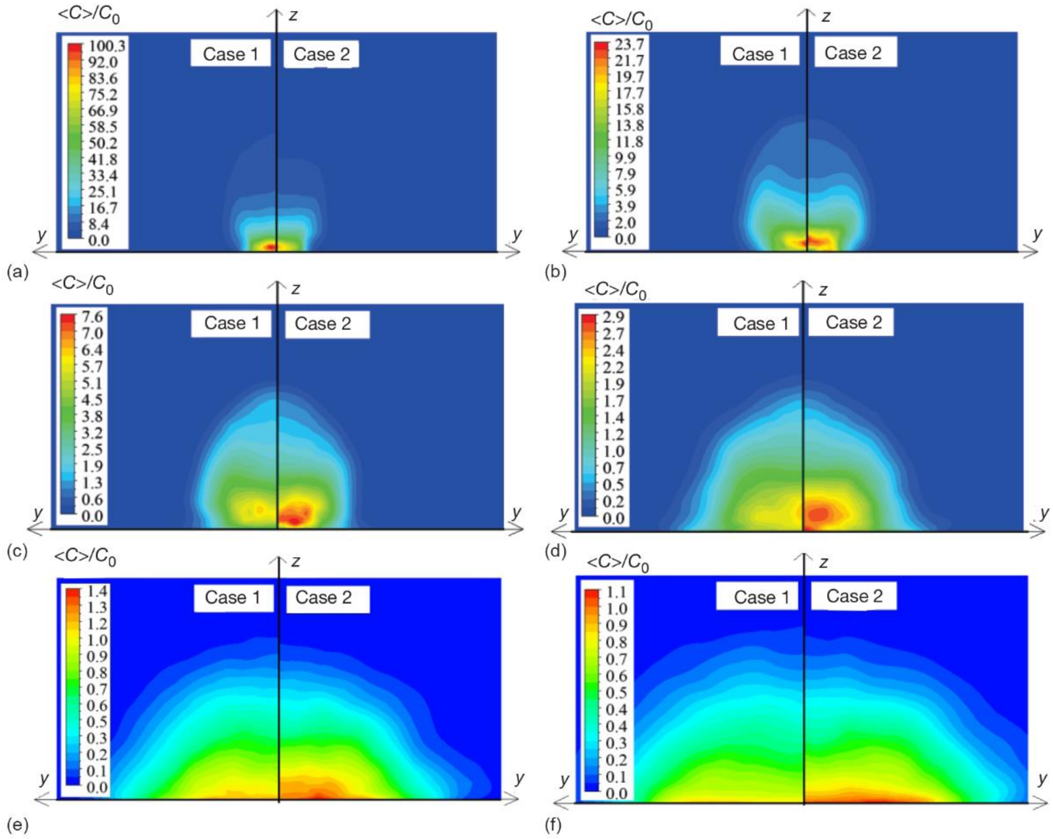

Figure 6. Mean tracer gas concentration $<C>/C_0$ calculated for Case 1 and Case 2 at cross-sections $x = 0.3125h$ (a), $0.625h$ (b);,h (c), $2h$ (d), $4h$ (e), and $6h$ (f)

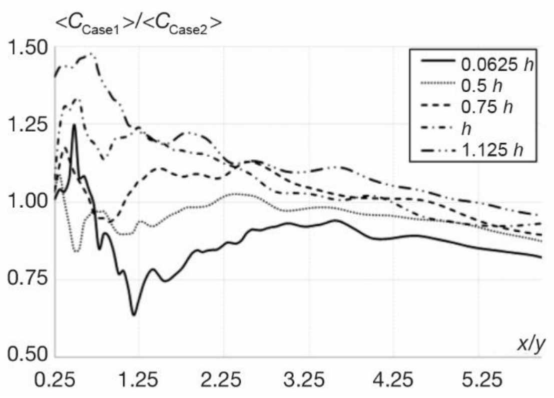

Figure 7. The ratio of the calculated mean tracer gas concentrations $<C_{\text{Case1}}>/<C_{\text{Case2}}>$, obtained along horizontal lines $z = 0.0625h$, $0.5h$, $0.75h$, h, and $1.125h$ at the central plane ($y = 0$ m)

for all the considered sections. At a height of $z/h = 1.125$ near the top of the prism, the mean pollutant concentration obtained for Case 1 is in ≈1.4 times higher than for the Case 2. At the heights of $0.75h$, h and $1.125h$, higher concentrations of pollutant also remains in the distance from the leeward side of the prism up to distances $x/h \approx 5$. Near the ground at a height of $0.0625h$ the ethylene concentration for Case 1 is lower ($<C_{\text{Case1}}>/<C_{\text{Case2}}> <1$) behind the injector, than for Case 2. For example, the ethylene concentration is $<C_{Case1}> \approx 0.64 <C_{Case2}>$ behind the injector (x/h = 1.25). This tendency is observed even far from the prism at $x > 5h$.

Conclusions

We conducted a series of numerical experiments to study dispersion of gas pollutant in a complex turbulent non-isothermal flow of atmospheric air around a prism with the parameter ratio 2:1:1 imitating a building. The main tool for numerical modelling was FLUENT 2020R1. We compared the URANS k-ω SST and IDDES k-ω SST approaches to the description of a turbulent flow of a mixture of gases on an experimental data [11]. The IDDES approach demonstrated good qualitative and quantitative correlation with the experimental data both in the velocity and the gas pollutant concentration profiles, as well as in the temperatures in the re-circulation zones on the top of the prism and behind it. These results demonstrate that the IDDES approach allows us to increase the precision of numerical modelling in comparison with URANS models. It should also be noted that both the approaches predict more intensive convection in the recirculation zone behind the prism as well as in the flow region above it.

We also compared the two heat regimes of the boundary-layer in the profiles of normalized gas pollutant concentration in the re-circulation zone behind the prism and in the distance behind the prism. We concluded that in the case of unstable thermal stratification (Ri_b = –0.085) a more intensive gas pollutant transfer to the leeward wall of the building is observed, the pollutant is transferred to the increased height above the prism and behind it, and pollutant concentration is lower on the ground in the distance behind the prism compared with a case of neutral (Ri_b = 0.0), close to an isothermal regime, stratification of the boundary-layer.

Acknowledgment

The research was supported by the Russian Science Foundation (project No. 20-79-00151).

References

[1] ***, WHO Global Air Quality Guidelines. Particulate Matter (PM2.5 and PM10), Ozone, Nitrogen Dioxide, Sulfur Dioxide and Carbon Monoxide, World Health Organization, Geneva, 2021
[2] Abbafati, C., *et al.*, Global Burden of 87 Risk Factors in 204 Countries and Territories, 1990-2019: A Systematic Analysis for the Global Burden of Disease Study, *Lancet*, *396* (2020), Oct., pp. 1223-1249
[3] Karagulian, F., *et al.*, Contributions to Cities' Ambient Particulate Matter (PM): A Systematic Review of Local Source Contributions at Global Level, *Atmos. Environ., 120* (2015), Nov., pp. 475-483
[4] Wang, Y., *et al.*, Spatiotemporal Variation and Source Analysis of Air Pollutants in the Harbin-Changchun (HC) Region of China During 2014-2020, *Environ. Sci. Ecotechnology*, *8* (2021), ID 100126
[5] Kim, Y., *et al.*, Multi Isotope Systematics of Precipitation to Trace the Sources of Air Pollutants in Seoul, Korea, *Environ. Pollut.*, *286* (2021), ID 117548
[6] Cheng, K., *et al.*, Understanding the Emission Pattern and Source Contribution of Hazardous Air Pollutants from Open Burning of Municipal Solid Waste in China, *Environ. Pollut., 263* (2020), ID 114417
[7] Minarro, M. D., *et al.*, A Multi-pollutant Methodology to Locate a Single Air Quality Monitoring Station in Small and Medium-size Urban Areas, *Environ. Pollut*., *266* (2020), ID 115279
[8] Mašić, A., *et al.*, Experimental Study of Temperature Inversions Above Urban Area Using Unmanned Aerial Vehicle, *Thermal Science, 23* (2018), 6A, pp. 3327-3338
[9] Vujić, B. B., *et al.*, Air Quality Monitoring and Modeling Near Coal Fired Power Plant, *Thermal Science*, *23* (2019), 6B, pp. 4055-4065
[10] Gromke, C., Ruck, B., Pollutant Concentrations in Street Canyons of Different Aspect Ratio with Avenues of Trees for Various Wind Directions, *Boundary-Layer Meteorol., 144* (2012), Feb., pp. 41-64

[11] Yoshie, R., *et al.*, Wind Tunnel Experimental Database of Air Pollution around a Building: Database on Indoor / Outdoor Air Pollution, Tokyo Polytechnic University, http://www.wind.arch.t-kougei.ac.jp/info_center/ pollution/Non-Isothermal_Flow.html
[12] ***, Urban Microclimate, ETH Zurich, https://carmeliet.ethz.ch/research/urban-microclimate.html
[13] Tsalicoglou, C., *et al.*, Non-Isothermal Flow Between Heated Building Models, *J. Wind Eng. Ind. Aerodyn.*, *204* (2020), ID 104248
[14] Zhao, Y., *et al.*, Buoyancy Effects on The Flows Around Flat and Steep Street Canyons in Simplified Urban Settings Subject to a Neutral Approaching Boundary-layer: Wind Tunnel PIV Measurements, *Sci. Total Environ.*, *797* (2021), ID 149067
[15] Zhao, Y., *et al.*, Isothermal and Non-Isothermal Flow in Street Canyons: A Review from Theoretical, Experimental and Numerical Perspectives, *Build. Environ.*, *184* (2020), ID 107163
[16] Franke J., *et al.*, *Best Practice Guideline for the CFD Simulation of Flows in the Urban Environment, COST Action 732*, Meteorological Institute, Blindeen, Oslo, Norvegia, 2007
[17] Tominaga, Y., *et al.*, AIJ Guidelines for Practical Applications of CFD to Pedestrian Wind Environment Around Buildings, *J. Wind Eng. Ind. Aerodyn.*, *96* (2008), 10-11, pp. 1749-1761
[18] Blocken, B., 50 Years of Computational Wind Engineering: Past, Present and Future, *J. Wind Eng. Ind. Aerodyn.*, *129* (2014), June, pp. 69-102
[19] Toparlar, Y., *et al.*, A Review on the CFD Analysis of Urban Microclimate, *Renew. Sustain. Energy Rev.*, *80* (2017), Dec., 1613-1640
[20] Liu, J., Niu, J. CFD Simulation of the Wind Environment around an Isolated High-rise Building: An Evaluation of SRANS, LES and DES Models, *Build. Environ.*, *96* (2016), Feb., pp. 91-106
[21] Valger, S. A., On Numerical Modeling of Aerodynamics of Urban Developments on Unstructured Computational Grids, *Thermophys. Aeromechanics*, *28* (2021), Dec., pp. 541-556
[22] Valger, S. A., *et al.*, Structure of Turbulent Separated Flow in the Neighborhood of a Plate-Mounted Prism of Square Section, *Thermophys. Aeromechanics*, *22* (2015), May, pp. 29-41
[23] Yoshie, R., *et al.*, Cooperative Project for CFD Prediction of Pedestrian Wind Environment in the Architectural Institute of Japan, *J. Wind Eng. Ind. Aerodyn.*, *95* (2007), 9-11, pp. 1551-1578
[24] Tominaga, Y., Flow Around a High-rise Building Using Steady and Unsteady RANS CFD: Effect of Large-scale Fluctuations on The Velocity Statistics, *J. Wind Eng. Ind. Aerodyn.*, *142* (2015), July, pp. 93-103
[25] Menter, F. R., *et al.*, Ten Years of Industrial Experience with the SST Turbulence Model Turbulence Heat and Mass Transfer, *Heat Mass Transf.*, *4* (2003), 1, pp. 625-632
[26] Shur, M. L., *et al.*, A Hybrid RANS-LES Approach with Delayed-DES and Wall-modelled LES Capabilities, *Int. J. Heat Fluid Flow*, *29* (2008), 6, pp. 1638-1649
[27] Strelets, M., Detached Eddy Simulation of Massively Separated Flows, *Proceedings*, 39th AIAA Aerospace Sciences, Reno, Nev, USA, pp. 1-18
[28] Travin, A., *et al.*, Physical and Numerical Upgrades in the Detached-Eddy Simulation of Complex Turbulent Flows, *Fluid Mech. its Appl.*, *65* (2004), Jan., pp. 239-254
[29] ***, Ansys Fluent Theory Guide, ANSYS Inc., USA, 2021
[30] Ramponi, R., Blocken, B., CFD Simulation of Cross-Ventilation for a Generic Isolated Building: Impact of Computational Parameters, *Build. Environ.*, *53* (2012), July, pp. 34-48
[31] Karava, P., *et al.*, Airflow Assessment in Cross-ventilated Buildings with Operable Façade Elements, *Build. Environ.*, *46* (2011), 1, pp. 266-279
[32] Spalart, P. R., *et al.*, A New Version of Detached-Eddy Simulation, Resistant to Ambiguous Grid Densities, *Theor. Comput. Fluid Dyn.*, *20* (2006), May, pp. 181-195
[33] Shur, M. L., *et al.*, Synthetic Turbulence Generators for RANS-LES Interfaces in Zonal Simulations of Aerodynamic and Aeroacoustic Problems, *Flow Turbulence and Combustion*, *93* (2014), May, pp. 63-92
[34] Tominaga, Y., Stathopoulos, T., Turbulent Schmidt Numbers for CFD Analysis with Various Types of Flowfield, *Atmos. Environ.*, *41* (2007), 37, pp. 8091-8099
[35] Lavruk, S. A., Valger, S. A., The Effect of Barrier Location on Characteristics of Gas Pollutant Transfer in the Vicinity of Highway, *Thermophys. Aeromechanics*, *28* (2021), Sept., pp. 369-381

Paper submitted: November 23, 2021
Paper revised: March 4, 2022
Paper accepted: March 14, 2022